

Scaling-Variable Distributions in High-Energy Inelastic Neutrino Interactions*

B. Aubert,[†] A. Benvenuti, D. Cline, W. T. Ford, R. Imlay, T. Y. Ling, A. K. Mann, F. Messing, J. Pilcher,[‡] D. D. Reeder, C. Rubbia, R. Stefanski, and L. Sulak

*Department of Physics, Harvard University, Cambridge, Massachusetts 02138, and
Department of Physics, University of Pennsylvania, Philadelphia, Pennsylvania 19174, and
Department of Physics, University of Wisconsin, Madison, Wisconsin 53706, and
Fermi National Accelerator Laboratory, Batavia, Illinois 60510*

(Received 1 August 1974)

We present measured distributions in the scaling variables x and y obtained from the reactions $\nu_\mu (\bar{\nu}_\mu) + \text{nucleon} \rightarrow \mu^- (\mu^+) + \text{hadrons}$ at high energy. The x distributions are consistent with scale invariance. The x and y distributions are used to perform the first test of charge-symmetry invariance in high-energy neutrino interactions, assuming the validity of scale invariance. A possible *effective* deviation from charge-symmetry invariance is observed, which could be the result of new particle production.

In a recent paper¹ we reported (i) a measurement of the total cross section for neutrino interactions, σ_ν , as a function of neutrino energy E_ν up to 150 GeV, and (ii) measurements of the ratio of the antineutrino to the neutrino total cross sections, $\sigma_{\bar{\nu}}/\sigma_\nu$, up to 70 GeV. Within experimental error, these results are consistent with $V-A$ coupling, Bjorken scale invariance,² and the spin- $\frac{1}{2}$ parton model.³ To test these ideas further at high energies, we present here the experimental distributions in the scaling variables $x = q^2/2ME_h$ and $y = E_h/E_\nu$ for neutrinos and antineutrinos, where $q^2 = 4E_\nu E_\mu \sin^2(\theta_\mu/2)$, E_h is the energy of the hadron cascade resulting from the neutrino-nucleon collision, and M is the nucleon mass. As before,¹ we identify positive- and negative-charged final-state muons with incident antineutrinos and neutrinos, respectively.

The experimental method was described earlier.^{1,4} Briefly, an enriched beam of neutrinos or antineutrinos at the Fermi National Accelerator Laboratory impinged on a pure-liquid-scintillator ionization calorimeter (target-detector) in which the neutrino-nucleon interaction occurred, and in which the hadron energy E_h was measured. The vector momentum of the emerging muon, p_μ , was measured in a magnetic spectrometer directly downstream of the target-detector. The energy of the incident neutrino was then computed from the sum $E_h + E_\mu$. Data were obtained with neutrino and antineutrino spectra generated in proton-nucleus collisions with proton energies E_p of 300 and 400 GeV.

Useful interactions took place in a fiducial region of the ionization calorimeter of cross-sectional area $2.4 \times 2.4 \text{ m}^2$ and length along the beam of 4.1 m. The total area and length of the ioniza-

tion calorimeter are $3 \times 3 \text{ m}^2$ and 7.2 m, respectively. Any event with $q^2 < 1.0 \text{ GeV}^2$ and $W < 1.6$ was eliminated from the scaling-variable distributions, where W is the invariant hadron mass. No separate cut on q^2 alone or on W alone was applied. The combined cut on q^2 and W eliminated quasielastic and Δ -production events,¹ and some inelastic events with $y < 0.1$ and neutrino (antineutrino) energy less than 30 GeV.

The energy response of the ionization calorimeter was calibrated with pions of known energies between 15 and 150 GeV incident on the front of the calorimeter. The measured response of the calorimeter at any energy within that interval is Gaussian with $\sigma = 12\%$. There is no evidence of a high-energy tail at the 1% level at any energy. A low-energy calibration point is provided by muons traversing the detector. The response of the muon spectrometer to muons of known momentum is approximately Gaussian with $\sigma \approx 15\%$ for any muon momentum less than about 80 GeV. These resolution functions, and also that for θ_μ , are included in the calculation of the expected scaling-variable distributions described below.

There are shown in Fig. 1 the directly observed distributions (histograms) in x for neutrinos and antineutrinos, combining data taken at 300 and 400 GeV. To exhibit the dependence on E_ν ($E_{\bar{\nu}}$), the distributions are plotted for two different regions of neutrino and antineutrino energy.⁵ For comparison we show also in Fig. 1 the corresponding x distributions calculated by assuming scale invariance and the simplifying relations among the nucleon structure functions, viz., $2xF_1(x) = F_2(x)$, $xF_3(x) = -F_2(x)$, and $F_i(x) = \bar{F}_i(x)$, where $\bar{F}_i(x)$ refers to antineutrino-nucleon scattering. We have also used the form of $F_2(x)$ ob-

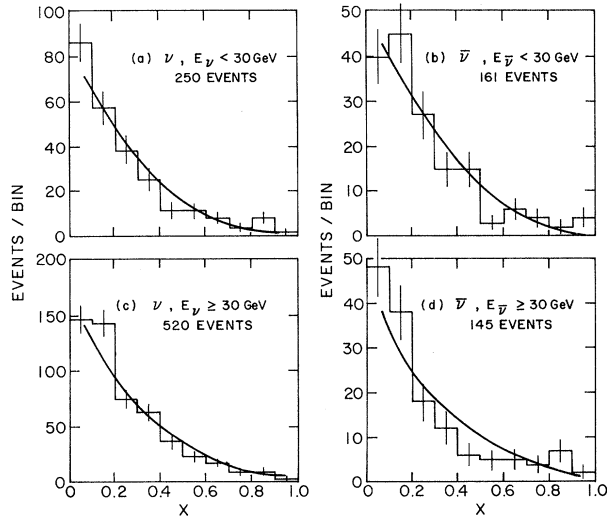


FIG. 1. Experimental distributions (histograms) in $x = q^2/2ME_h$ and calculated distributions (solid lines) expected from scale invariance using $F_2(x)$ from electroproduction and simplifying relations among the structure functions (see text).

tained from electroproduction experiments⁶ (for $x \gtrsim 0.1$), and included incident neutrino and antineutrino spectra¹ and the geometric detection efficiency of the apparatus^{4,7} in obtaining the calculated distributions, which are compared with the uncorrected experimental distributions, both normalized to the same area.

The shapes of the observed and calculated x distributions in Fig. 1 indicate that the x distributions for neutrinos and antineutrinos are essentially the same, and are not significantly dependent on E_ν ($E_{\bar{\nu}}$). In Fig. 2 are plotted the measured y distributions for neutrinos and antineutrinos in the same regions of E_ν ($E_{\bar{\nu}}$) as before, with the calculated distributions included for comparison. The observed x and y distributions for neutrinos are consistent with the complex of as-

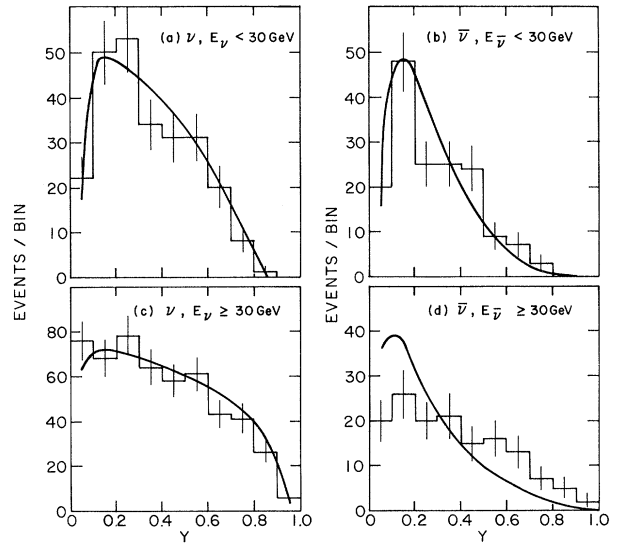


FIG. 2. Experimental and calculated distributions (assuming $B=1$) in $y = E_h/E_\nu$. The falloff in the first bin in y in (a) and (b) is due to the joint selection criterion $W > 1.6$ GeV and $q^2 > 1.0$ GeV².

sumptions that enter the calculated distributions, and with earlier data.^{8,9}

The y distributions for antineutrinos, however, are not completely consistent with the simplest form expected from lower-energy ($3 < E_{\bar{\nu}} < 10$ GeV) data,⁸ viz., $dN/dy \sim (1-y)^2$. For $E_{\bar{\nu}} < 30$ GeV [Fig. 2(b)], the experimental y distribution is not in evident disagreement with that form, but for $E_{\bar{\nu}} > 30$ GeV [Fig. 2(d)], the observed y distribution has 43 events with $y > 0.5$ out of a total of 145, i.e., $(30 \pm 5)\%$, whereas $(1-y)^2$ multiplied by the detection efficiency predicts less than 10%.

A somewhat more general analysis of the y distributions may be made by relaxing the assumptions $x\bar{F}_3(x) = -F_2(x)$ and $2xF_1(x) = F_2(x)$. We write the scale-invariant differential cross section for inelastic neutrino (antineutrino)-nucleon collisions in the form

$$d^2\sigma^{\nu\bar{\nu}}/dx dy = (G^2ME_\nu/\pi)F_2(x)[1 - y(1 \mp B^{\nu\bar{\nu}}) + \frac{1}{2}y^2(1 \mp B^{\nu\bar{\nu}}) + \frac{1}{2}y^2R_L^{\nu\bar{\nu}}], \quad (1)$$

where the upper signs are to be taken for neutrinos, $B^\nu = -xF_3(x)/F_2(x)$, $R_L^\nu = [2xF_1(x) - F_2(x)]/F_2(x)$, and $B^{\bar{\nu}} = -x\bar{F}_3(x)/\bar{F}_2(x)$, etc. From the positivity conditions, $|xF_3(x)| \leq 2xF_1(x) \leq F_2(x)$, it follows that $R_L \leq 0$, and therefore the term in R_L cannot contribute to the excess of events observed at $y > 0.5$. With $R_L = 0$, Eq. (1) is equivalent to a parametrization which mixes a y -independent term and a $(1-y)^2$ term in arbitrary proportions.

With the assumption that charge-symmetry in-

variance holds, the ratio of antineutrino to neutrino cross sections integrated over all x and y is $\sigma^{\bar{\nu}}/\sigma^\nu = (2 - \bar{B})/(2 + \bar{B})$, where \bar{B} is the average value of $B(x)$. One obtains $\bar{B} = 0.9 \pm 0.2$ from the ratio $\sigma^{\bar{\nu}}/\sigma^\nu = 0.37 \pm 0.1$ measured¹ at a mean energy of about 40 GeV, and $\bar{B} \approx 0.85$ at lower neutrino energies.⁸

The dependence on x of the y distributions has been investigated by partitioning the data of Fig.

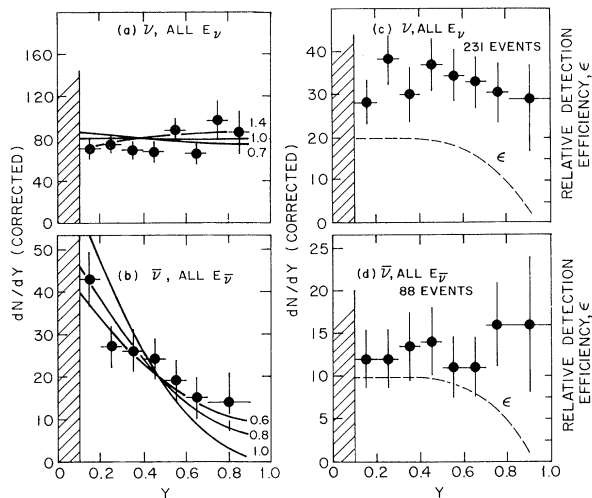


FIG. 3. Corrected experimental y distributions (a) and (b) for the region $0.6 > x \geq 0.1$, and (c) and (d) for the region $x < 0.1$. Points at $y = 0.05$ are omitted because they are sensitive to resolution corrections. Points at $y = 0.95$ in (a) and (b) are omitted because they are sensitive to efficiency corrections. Calculated curves for different values of B^ν and $B^{\bar{\nu}}$ are also shown in (a) and (b).

2 between the regions $x < 0.1$ and $x \geq 0.1$. We have also divided the data by the relative detection efficiency to display the corrected experimental distributions. The results for $0.6 > x \geq 0.1$ for neutrinos and antineutrinos are shown in Figs. 3(a) and 3(b), where it is seen that the excess of events at high y in the antineutrino distribution has largely disappeared. In Figs. 3(c) and 3(d) are shown the corrected y distributions for neutrinos and antineutrinos in the $x < 0.1$ region. Note the striking difference between the antineutrino y distributions in the two x regions.

Apart from resolution effects that influence the lowest bin in y , the experimental distributions in Figs. 3(a) and 3(b) are fitted by Eq. (1) with the values $B^\nu = 1.4 \pm 0.6$ and $B^{\bar{\nu}} = 0.6 \pm 0.2$, which are consistent with the value of \bar{B} given above. The y distributions of Figs. 3(c) and 3(d), however, yield $B^\nu = 1.3 \pm 0.6$ and $B^{\bar{\nu}} = -1.2^{+0.8}_{-1.3}$.

If charge symmetry is assumed, $B(x)$ can be determined by using Eq. (1) for each value of x from the ratios of antineutrino and neutrino cross sections integrated over all y . The x distributions in Fig. 1 were combined, corrected for detection efficiency, and normalized to the value $\sigma^{\bar{\nu}}/\sigma^\nu = 0.37$. The results are shown in Fig. 4 where it is seen that $B(x)$ is constant within experimental error over the entire x range, $x < 0.5$.

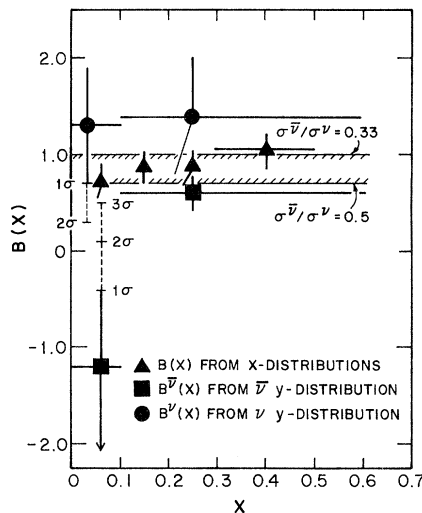


FIG. 4. Plot of the values of $B(x)$, $B^\nu(x)$, and $B^{\bar{\nu}}(x)$ obtained from the experimental x and y distributions in the regions $x < 0.1$ and $0.6 > x \geq 0.1$. The three points in the $x < 0.1$ region, all of which should be plotted at $x = 0.05$, are shifted slightly with respect to each other for improved clarity.

These results are statistically insensitive to the possible decrease of $B(x)$ at very small x conjectured in the parton model.

To test charge-symmetry invariance, we compare the values of B determined separately from x and y distributions and total cross section measurements. In Fig. 4 are shown, in addition to the values of $B(x)$ from the x distributions, the four values of $B^\nu(x)$ and $B^{\bar{\nu}}(x)$ obtained from the four y distributions of Fig. 3. Charge-symmetry invariance requires that $B^{\bar{\nu}}(x) = B^\nu(x) = B(x)$. In the region $0.6 > x \geq 0.1$, there is agreement within 1 standard deviation among the various measured values of B^ν , $B^{\bar{\nu}}$, and $B(x)$, indicating that the data are not inconsistent with charge symmetry. In the region $x < 0.1$, the measured value of $B^{\bar{\nu}}$ differs from the separately determined values of B^ν and $B(x)$ by about 3 standard deviations.

We summarize these results as follows. The close similarity of the structure function $F_2(x)$ observed in both electron and neutrino deep inelastic scattering, up to a neutrino energy of about 150 GeV (Fig. 1), and the consistency of the y distributions in the region $0.6 > x \geq 0.1$ [Figs. 3(a) and 3(b)] are further substantive confirmation of scale invariance. In that x region, the approximate equality of the values of $B^\nu(x)$, $B^{\bar{\nu}}(x)$, and $B(x)$ normalized by means of $\sigma^{\bar{\nu}}/\sigma^\nu$ constitute evidence for charge-symmetry invariance. On the other hand, in the region $x < 0.1$ the excess of

events at high y in the antineutrino y distribution leads to a value of B^{ν} different from the values of B^{ν} and $B(x)$, which is suggestive of an *effective* deviation from charge symmetry if the validity of scale invariance is assumed. This may arise in part from new particle production or from an anomalously large cross section for direct strange-particle production.¹⁰ Note that new particle production tends for kinematic reasons to populate preferentially the regions of small x and large y .¹¹

It is a pleasure to acknowledge the aid and encouragement of the Fermi National Accelerator Laboratory staff. We thank D. Cheng and R. L. Piccioni for their early contributions to this work. We have profited from discussions with Professor S. B. Treiman.

*Work supported in part by the U. S. Atomic Energy Commission.

†On leave of absence from the Laboratoire de l'Accélérateur Linéaire, Orsay, France.

‡Alfred P. Sloan Foundation Fellow, now at the University of Chicago, Chicago, Ill. 60637.

¹A. Benvenuti *et al.*, Phys. Rev. Lett. **32**, 125 (1974), and in Proceedings of the Seventeenth International Conference on High Energy Physics, London, England, 1–10 July 1974 (to be published).

²J. D. Bjorken, Phys. Rev. **179**, 1547 (1969); J. D.

Bjorken and E. A. Paschos, Phys. Rev. D **1**, 3151 (1970).

³R. P. Feynman, Phys. Rev. Lett. **23**, 1415 (1969), and in *Proceedings of the Third Topical Conference on High Energy Collisions, Stony Brook, New York, 1969*, edited by C. N. Yang *et al.* (Gordon and Breach, New York, 1970); J. D. Bjorken and E. A. Paschos, Phys. Rev. **185**, 1975 (1969).

⁴A. Benvenuti *et al.*, Phys. Rev. Lett. **30**, 1084 (1973).

⁵The energy regions into which the data are divided are, to some extent, arbitrary. However, no significant change is made in the results if the data are cut at 25, 40, or 50 GeV. Above 50 GeV, the antineutrino sample becomes statistically limited.

⁶G. Miller *et al.*, Phys. Rev. D **5**, 528 (1972).

⁷A. Benvenuti *et al.*, Phys. Rev. Lett. **32**, 800 (1974); B. Aubert *et al.*, Phys. Rev. Lett. **32**, 1454 (1974).

⁸See, for example, D. H. Perkins, in *Proceedings of the Fifth Hawaii Topical Conference on Particle Physics*, edited by P. N. Dobson, Jr., V. Z. Peterson, and S. F. Tuan (University of Hawaii, Honolulu, 1973); T. Eichten *et al.*, Phys. Lett. **B46**, 274, 281 (1973).

⁹B. C. Barish *et al.*, Phys. Rev. Lett. **31**, 565 (1973).

¹⁰S. L. Glashow, J. Iliopoulos, and L. Maiani, Phys. Rev. D **2**, 1285 (1970); A. de Rújula, H. Georgi, S. L. Glashow, and H. R. Quinn, to be published; G. Altarelli, N. Cabibbo, L. Maiani, and R. Petronzio, CERN Report No. TH-1757, (to be published).

¹¹S. L. Adler, NAL Report No. 74/39 TH (to be published); D. Cline, in Proceedings of the Fourth International Conference on Neutrino Physics and Astrophysics, Philadelphia, 26–28 April 1974 (to be published); M. K. Gaillard, NAL Report No. FN-259, 1974 (unpublished).

Resonance Pole with $J^P = \frac{3}{2}^+$ in a Coupled-Channel Analysis of K^+p Elastic Scattering Data

Richard A. Arndt, Roger H. Hackman, and L. David Roper

Virginia Polytechnic Institute and State University, Blacksburg, Virginia 24061

and

Phillip H. Steinberg *

University of Maryland, College Park, Maryland 20742

(Received 1 April 1974)

Energy-dependent partial-wave amplitudes based on a coupled-channel ($K^+p, K\Delta$) K -matrix formalism are obtained for elastic K^+p scattering up to $P_{lab} = 2$ GeV/ c . The data used include new high-precision differential cross sections. A total of 42 parameters describing the $l \leq 4$ partial waves are used to fit 3822 data points and the best solution found has a χ^2 per degree of freedom of 1.33. This solution exhibits a T -matrix Z^* resonance pole in the P_3 partial wave with mass coordinates $1787 - i100$ MeV.

In recent years there has been considerable effort invested in the measurement and analysis of elastic K^+p scattering to determine whether the bump in the total cross section at $P_{lab} = 1.2$ GeV/ c can be interpreted as a Z^* resonance.¹ Most

analyses to date have been basically of the single-energy type, an Argand trajectory being determined by selectively connecting single-energy solutions at adjoining energies by means of a "shortest-path" criterion. Although there have